Journal of Advanced Marine Engineering and Technology, Vol. 49, No. 1, pp. 20~28, 2025
J. Advanced Marine Engineering and Technology (JAMET)
https://doi.org/10.5916/jamet.2025.49.1.20

ISSN 2234-7925 (Print)
ISSN 2765-4796 (Online)
Original Paper

Design of cathodic protection potentials and impressed current densities in ICCP systems for ships with coating defects

Uijun Kim[1] · Nayoung Kim[2] · Joonhyu Shin[3] · Yoonsung Maeng[4] · Seunghyo Lee†

(Received February 17, 2025 ; Revised February 24, 2025 ; Accepted February 25, 2025)

Abstract: ICCP is commonly applied to ships in combination with coatings to prevent corrosion; however, coating failures increase current demand. Therefore, understanding the relationship between ICCP and coating defects is essential for optimizing ICCP system under practical operating conditions. This study identifies the optimal cathodic protection potentials, considering coating defect rates as a key variable. Furthermore, the impressed current densities for the cathodic potentials were calculated, measured, and simulated. The coefficients of determination of 0.996 and 0.962 for the simulation and experimental results, respectively, indicate a strong correlation, demonstrating that the obtained values were highly consistent. The comparison suggests that minor discrepancies arose due to the formation of oxide films during potentiostatic tests. The assessment of cathodic potential effectiveness confirmed that -0.7 V also provided excellent protective performance. This study provides insights into ICCP operation and design strategies for practical operating conditions through electrochemical tests, computer simulation, and material characterization.

Keywords: ICCP, Cathodic protection potential, Impressed current density, Ships with coating defects

1. Introduction

Ships are composed of various components, such as hull, propeller, and rudder, each utilizing different metals depending on their function and operating environment. All metals exhibit potential differences relative to other metals, and when a ship is exposed to seawater, an infinite electrolyte, an electrochemical cell forms, consisting of an anode, cathode, electrolyte, and closed circuit, leading to galvanic corrosion. In particular, the steel used for the ship's hull and the nickel-aluminum-bronze (Ni-Al-Bronze, NAB) alloy used for the propeller have potentials of -0.60 V vs. Ag/AgCl and -0.25 V vs. Ag/AgCl, respectively, in seawater. As a result, the hull acts as the anode and undergoes corrosion **[1]**.

To prevent corrosion, cathodic protection (CP) is commonly applied to ships. According to National Association of Corrosion Engineers (NACE), cathodic protection is defined as "a technique to reduce corrosion of a metal surface by making that surface the cathode of an electrochemical cell" **[2]**. Ships typically employ two CP methods: galvanic cathodic protection and impressed current cathodic protection (ICCP). Galvanic cathodic protection prevents hull corrosion by attaching a sacrificial metal with a more negative potential than the hull thereby inhibiting anodic reactions on hull surface. However, this method has limitations, including non-uniform potential distribution due to the ship's geometry, a restricted protection range, very high dimensional tolerances, and challenges in maintenance and long-term effectiveness **[3]**. Due to these reasons, ICCP has become the preferred cathodic protection method for ships.

ICCP suppresses corrosion by directly supplying current to the hull from an external power source, polarizing the hull to a low potential. As the supplied current increases, the potential of the hull surface shifts more negatively, inhibiting anodic dissolution

† Corresponding Author (ORCID: http://orcid.org/0000-0002-7960-2906): Associate Professor, Department of Ocean Advanced Materials Convergence Engineering, Korea Maritime & Ocean University, 727, Taejong-ro, Yeongdo-gu, Busan 49112, Korea, E-mail: lsh@kmou.ac.kr, Tel: +82-51-410-4352

1 Ph. D. Candidate, Department of Ocean Advanced Materials Convergence Engineering, Korea Maritime & Ocean University, E-mail: uijun95@g.kmou.ac.kr, Tel: +82-51-410-4968

2 Undergraduate Student, Department of Ocean Advanced Materials Convergence Engineering, Korea Maritime & Ocean University, E-mail: kny5501@g.kmou.ac.kr, Tel: +82-51-410-4968

3 Researcher, Power Electronics Research, Research & Development Division, VICTEK, E-mail: tlswnsgb11@victek.co.kr, Tel: +82-70-4355-4012

4 Researcher, Power Electronics Research, Research & Development Division, VICTEK, E-mail: maengys@victek.co.kr, Tel: +82-70-7162-3820

and reducing the corrosion rate. According to the NACE RP 0775, maintaining average corrosion rate less than 0.025 mm/yr was suggested for qualitatively low carbon steel corrosion rate **[4]**.

ICCP, when used alone, requires a significant amount of current for corrosion protection, making it economically inefficient. Hence, it is typically applied to ships in combination with coatings. However, coating failures are inevitable due to inherent defects, progressive damage sustained during operation, and contamination on the substrate beneath the coating. One of the major challenges in designing ICCP systems is the gradual deterioration of coatings over time. Since the extent of coating deterioration can only be assessed through inspection after the system is taken out of service, ICCP systems are designed without considering the presence of the coating. This ensures corrosion protection even in the worst-case scenario of complete coating failure. While this design guarantees sufficient power availability, it may also lead to excessive overdesign, resulting in increased operational costs. The damaged areas require higher current to prevent corrosion. In addition, the increased current demand also induces underwater electric potential signals, which can be exploited for ship tracking in military applications **[5]**. Therefore, understanding the relationship between coating defects and the distribution of potential and current is essential for optimizing ICCP system performance.

Although numerous studies have investigated ICCP systems for corrosion protection in marine environments, relatively little attention has been given to electrochemical techniques such as potentiodynamic polarization and electrochemical impedance spectroscopy (EIS) for precise determination of protection potential. Furthermore, studies incorporating material characterization methods to analyze surface and interface phenomena under ICCP conditions remain limited **[6]-[8]**.

In this study, we determine the optimal cathodic protection potential and impressed current density in ICCP systems for ships with coating defects. Corrosion behaviors and impressed current density for cathodic potentials were investigated through electrochemical experiments and computer simulations. In addition, material characterization was performed to verify the effectiveness of the suggested cathodic protection potentials. This integrated approach provides deeper insights into the effectiveness and reliability of cathodic protection potentials and impressed current densities in ICCP systems.

2. Experiments

2.1 Materials

SS400 steel, commonly used for ship hulls, was used as specimens. The chemical composition (wt%) is as follow: C (0.18), Si (0.14), Mn (0.71), P (0.013), S (0.006), with Fe as the balance. Prior to testing, the specimens were sequentially abraded with SiC sandpapers up to 600 grit, rinsed with deionized water and ethanol, and airdried under ambient conditions. To ensure a consistent surface oxide film, all specimens were prepared within 10 minutes before electrochemical testing. The exposed surface area of the specimens was controlled using NITTOFLON 903 PTFE tape, which has outstanding electrical insulation properties and excellent chemical resistance, to replicate coating defects at levels of 10, 30, 50, and 100% and the specimens were designated as Coating Defect_10% (CD10%), Coating Defect_30% (CD30%), Coating Defect_50% (CD50%), and Coating Defect_100% (CD100%), respectively.

2.2 Electrochemical Tests

The effect of coating defects on the current distribution in cathodic protection systems in seawater was investigated through potentiodynamic polarization, potentiostatic, and EIS. All electrochemical tests were conducted using a potentiostat in a three-electrode system, comprising a Pt wire as the counter electrode, an Ag/AgCl electrode as the reference, and the specimen as the working electrode.

Potentiodynamic polarization tests were conducted to evaluate the intrinsic electrochemical behavior under varying coating defect conditions in a potential range of -1.0 to 0 V vs. Ag/AgCl at a scan rate of 0.166 mV/s in 3.5 wt% NaCl solution. EIS measurements were performed at E_{corr}, E_{NACE}, -0.7, and -0.8 V vs. Ag/AgCl across a frequency range of 100 kHz to 0.01 Hz, using a sinusoidal voltage with an amplitude 10 mV, to analyze surface characteristics and assess compliance with cathodic protection criteria (E_{corr} and E_{NACE} is determined based on the results and defined in Section 3.2). The EIS data were fitted to an appropriate equivalent circuit model using Gamry Echem Analyst software. Additionally, potentiostatic tests were conducted to simulate impressed current conditions, with the specimens cathodically polarized at -0.8 V vs. Ag/AgCl under simulated damaged coating conditions for 24 h. To ensure reproducibility, all tests were conducted at least three times.

2.3 Computer Simulation

Numerical simulations were performed using the finite element method (FEM) in COMSOL Multiphysics to analyze the distribution of current densities on ship's hull. The ship model was constructed using the ship drawings provided by COMSOL **[9]**. The model was designed with dimensions of approximately 35 m in length, 5.7 m in width, and 5 m in height for the submerged portion. The anode was positioned 8 meters from the stern. Electrochemical reactions were incorporated into the simulation by applying realistic polarization curve data as boundary conditions. The polarization curve for steel was assigned to the ship's hull. The primary electrode reaction occurring on the metal surface is oxygen reduction. As the transport of oxygen in the seawater is restricted by its diffusion rate to the surface, the current density is constrained to 5 A/m^2 based on electrode kinetics. Consequently, the local current density can be expressed as follows:

$$i_{loc} = \frac{i_{lim} \cdot i_{kin}}{i_{lim} + |i_{kin}|}$$

Where i_{lim} represents the diffusion-limited current density and i_{kin} accounts for the electrode kinetics.

All simulations assumed seawater with an electrical conductivity of σ = 4.5 S/m to replicate real seawater conditions. Additionally, an Ag/AgCl reference electrode was used to determine the protective potential. This setup enables a precise evaluation of the electrochemical behavior and the spatial distribution of potential and current across the ship's surface under varying conditions.

2.4 Characterization

To assess the effectiveness of the cathodic protection potentials, scanning electron microscopy (SEM) combined with energy-dispersive spectroscopy (EDS) was employed to examine the surface morphology and chemical composition. The SEM/EDS analysis was performed at an accelerating voltage of 15.0 kV.

3. Results and Discussion

3.1 Corrosion of Ship's Hull with Coating Defects

Potentiodynamic tests were conducted to investigate the electrochemical properties of a ship's hull with damaged coatings. From the polarization curves, electrochemical parameters, such as corrosion potentials (E_{corr}), corrosion current densities (i_{corr}), anodic Tafel slope (β_a), and cathodic Tafel slope (β_c), were obtained using EC-Lab software. **Figure 1** presents the polarization curves for coated steels with damages, while the electrochemical parameters derived from these tests are summarized in **Table 1**. The slight variations in E_{corr} were attributed to the formation of oxide films during the potentiodynamic tests, though they remained within the range of -400 to -500 mV. In addition, the corrosion current densities increased with increased coating defects due to the enlarged areas for electrochemical reactions. On the other hand, since the tested specimens were composed of the same material and subjected to identical conditions, the kinetics of anodic and cathodic reactions were found to be similar. The obtained β_a and β_c values were approximately 75 mV/decade and 635 mV/decade, respectively.

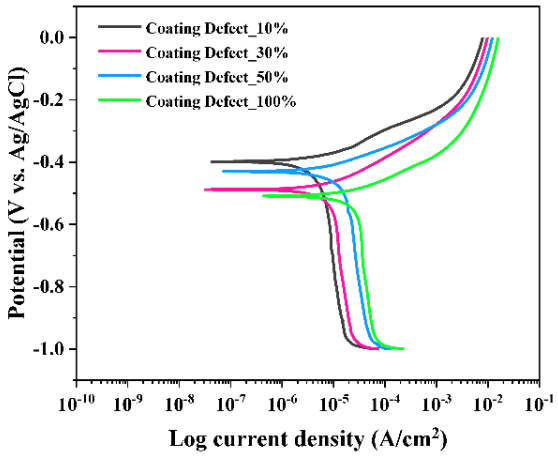

Figure 1: Potentiodynamic polarization curves of coated steel as a function of coating defects in 3.5 wt% NaCl solution

Table 1: Electrochemical parameters obtained from the potentiodynamic polarization tests under different coating defect conditions in 3.5 wt% NaCl solution

Coating defects	E_{corr} ($V_{Ag/AgCl}$)	i_{corr} (μA/cm^2)	β_a (mV/dec.)	β_c (mV/dec.)	Corrosion rate (mm/yr)
Coating Defect_10%	-400.085	4.327	74.0	654.1	0.050
Coating Defect_30%	-481.814	6.683	77.5	650.7	0.078
Coating Defect_50%	-426.773	11.847	75.1	614.5	0.137
Coating Defect_100%	-507.755	20.270	75.6	623.3	0.235

Table 2: Calculated applied current densities for cathodic protection and corrosion rates at the potentials as a function of coating defect levels

Coating defects	E_{corr}	E_{NACE}			-0.7 V		-0.8 V	
	Corrosion rate (mm/yr)	Potential (V)	i_{cp} (μA/cm^2)	Corrosion Rate (mm/yr)	i_{cp} (μA/cm^2)	Corrosion Rate (mm/yr)	i_{cp} (μA/cm^2)	Corrosion Rate (mm/yr)
Coating Defect_10%	0.050	-0.42	0	0.025	9.25	4.06×10^{-12}	11.31	1.81×10^{-13}
Coating Defect_30%	0.078	-0.52	3.96	0.025	12.81	1.20×10^{-10}	15.71	7.02×10^{-13}
Coating Defect_50%	0.137	-0.48	10.87	0.025	26.81	3.23×10^{-11}	32.26	1.50×10^{-12}
Coating Defect_100%	0.235	-0.58	27.44	0.025	36.15	6.65×10^{-10}	43.36	3.16×10^{-11}

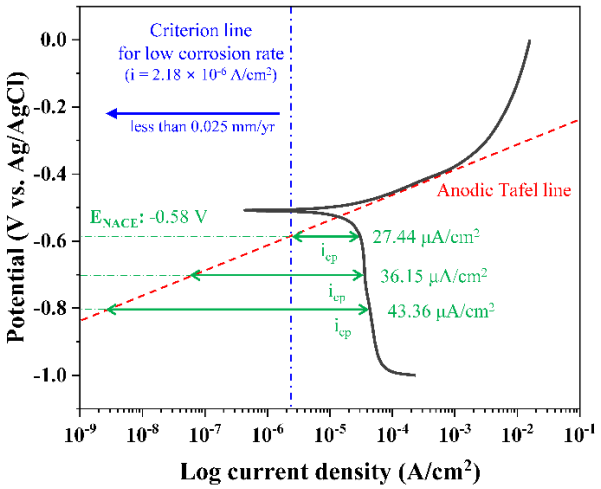

Figure 2: Calculated applied current density for cathodic protection (i_{cp}) and the anodic Tafel line of CD100% derived from the potentiodynamic polarization curve

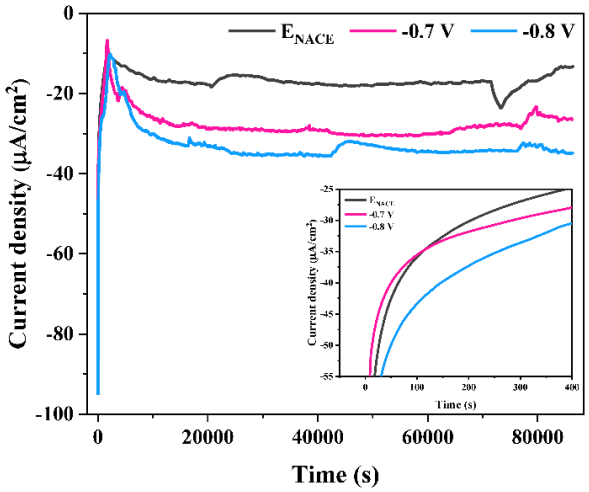

Figure 3: Records of applied current densities of CD100% during potentiostatic tests conducted at E_{NACE}, -0.7 V, and -0.8 V in 3.5 wt% NaCl solution

To evaluate the severity of corrosion in the damaged areas, corrosion rates were calculated based on Faraday's law using the following equation:

$$\text{Corrosion rate (mm/yr)} = \frac{0.00327 \times a \times i}{n \times D}$$

where a is the atomic weight, i is the corrosion current density, n is the number of electrons transferred per metal atom, and D is the density of the metal. As shown in **Table 1**, the corrosion rates of CD10%, CD30%, CD50%, and CD100% were 0.050, 0.078, 0.137, and 0.235 mm/yr, respectively. These values exceed the low corrosion rate threshold (0.025 mm/yr) recommended by NACE, indicating the necessity of implementing ICCP systems to mitigate corrosion.

3.2 Investigation on Cathodic Protection Potential and Impressed Current Density

According to the international standard ISO 12473: General Principles of Cathodic Protection in Seawater, the recommended cathodic protection potential range is -0.8 to -1.1 V vs. Ag/AgCl [10]. To minimize the required current density for cathodic protection (i_{cp}), the lowest cathodic potential that satisfies the NACE criterion for low corrosion rates (E_{NACE}) was determined from polarization curves. **Figure 2** presents the potentiodynamic polarization curve, anodic Tafel line, and i_{cp} for each cathodic potential. CD100% was presented as a representative. The E_{NACE} was calculated to be -0 .58 V. additionally, 27.44, 36.15, and 43.36 μA/cm^2 of current densities were required to maintain the potential of CD100% at -0.58, -0.7, and -0.8 V, respectively. The corresponding corrosion rates were reduced to 0.025, 6.65×10^{-10}, and 3.16×10^{-11} mm/yr, indicating that -0.58 and -0.7 V could also be considered effective cathodic protection potentials. Other calculated applied current densities and corrosion rates are summarized in **Table 2**.

Potentiostatic tests were performed to replicate ICCP-applied environments and validate the calculated i_{cp} values, assessing the applicability to ICCP conditions. **Figure 3** presents the recorded current densities of CD100% during the tests. Impressed current

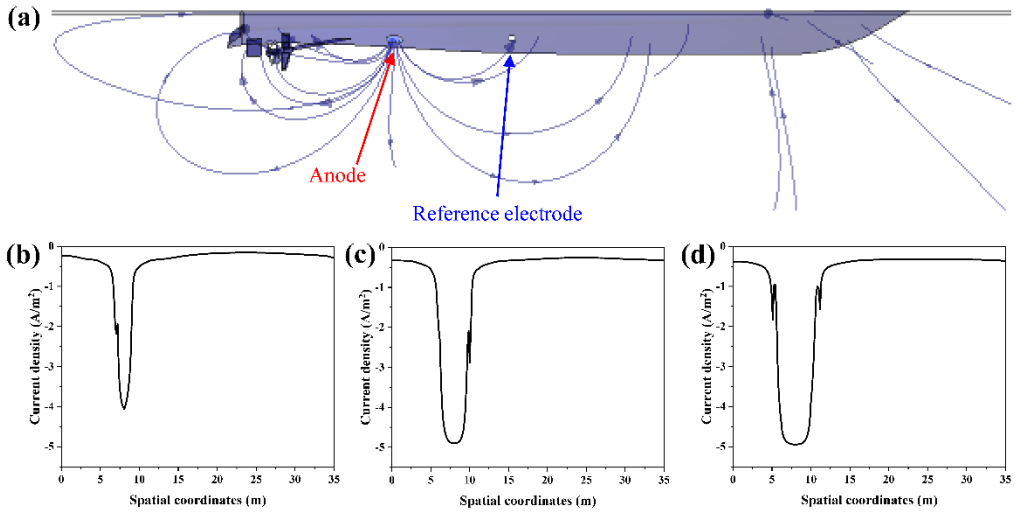

Figure 4: (a) Computational model of the current density distribution on a ship with CD100% hull and the corresponding i_{cp} values across the hull at cathodic potentials of (b) E_{NACE}, (c) -0.7 V, and (d) -0.8 V

densities initially decreased sharply due to the formation of oxide films, which reduced the active surface area, as shown in the inset. However, as the oxide films continued to grow, their low electrical conductivity led to an increase in the required impressed current density. After around 20,000 s, the surface of CD100% stabilized, requiring 17.50, 29.62, and 34.30 μA/cm^2 of i_{cp} at E_{NACE}, -0.7, and -0.8 V, respectively.

To simulate i_{cp} on ICCP-applied ships under different cathodic potentials, which is challenging to measure in full-scale experiments, COMSOL Multiphysics was employed. **Figure 4(a)** presents a 3D simulation of the current density distribution at a cathodic protection potential of -0.8 V, while **Figure 4(b), (c),** and **(d)** illustrate the required i_{cp} values across the hull under cathodic potentials of E_{NACE}, -0.7, and -0.8 V, respectively. In the ship modeling, the position and number of anodes were not optimized, resulting in a high current density near the 8 m region where the anodes are located. Hence, the current density values obtained from the simulation were selected from a spatial coordinate where the potential was stably maintained to establish the cathodic potential. The acquired impressed current densities at E_{NACE}, -0.7, and -0.8 V were 27.84, 33.68, and 39.76 μA/cm^2, respectively.

The calculated, measured, and simulated i_{cp} at E_{NACE}, -0.7, and -0.8 V were summarized in **Table 3** and the trend lines and coefficient of determination (R^2) are presented in **Figure 5**. The R^2 was calculated based on the square of the Pearson correlation coefficient. When the trend line was plotted based on the calculated values, the simulation and experimental results exhibited high R^2 of 0.996 and 0.962, respectively. The experimentally obtained

Table 3: Calculated, experimental, and simulated applied current densities for cathodic protection of CD100% as a function of cathodic protection potentials

	E_{NACE} (-0.58 V)	-0.7 V	-0.8 V
Calculation (μA/cm^2)	27.44	36.15	43.36
Experiments (μA/cm^2)	17.50	29.62	34.30
Simulation (μA/cm^2)	27.84	33.68	39.76

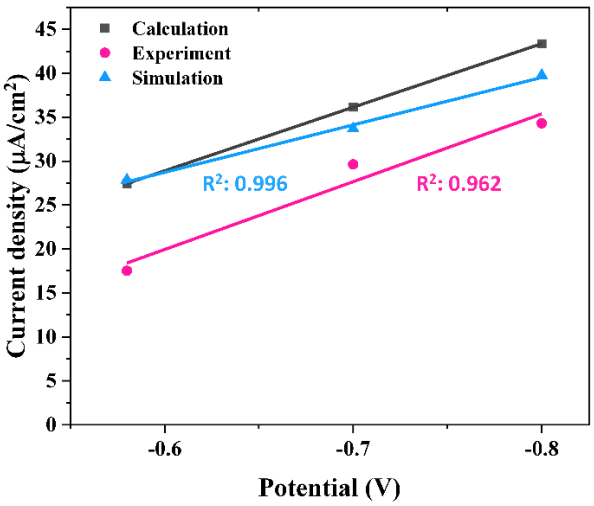

Figure 5: Trend line and R^2 values of the calculated, measured, and simulated i_{cp} for cathodic protection of CD100% at E_{NACE}, -0.7 V, and -0.8 V of cathodic protection potentials

current density was lower than the calculated and simulated values, likely due to the lengthy duration of the potentiostatic tests. As observed in the potentiostatic tests, a higher current density was initially required before stabilizing over time, suggesting

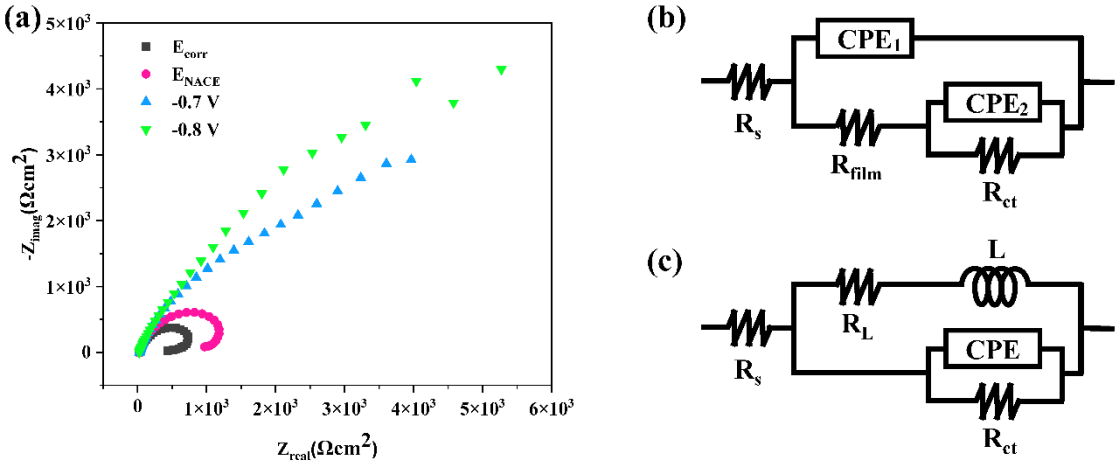

Figure 6: (a) Nyquist plots of CD100% at cathodic protection potentials of E_{corr}, E_{NACE}, -0.7 V, and -0.8 V and equivalent circuits of CD100% at (b) E_{corr} and E_{NACE} and (c) -0.7 V and -0.8 V

Table 4: Impedance parameters of CD100% at cathodic protection potentials of E_{corr}, E_{NACE}, -0.7 V, and -0.8 V

Cathodic Potential	R_s ($\Omega \cdot cm^2$)	R_L ($\Omega \cdot cm^2$)	L (H cm^2)	R_{film} ($\Omega \cdot cm^2$)	n	C_{film} ($\mu F/cm^2$)	R_{ct} ($\Omega \cdot cm^2$)	n	C_{dl} ($\mu F/cm^2$)	R_{total} ($\Omega \cdot cm^2$)
E_{corr}	27.2	1550.9	78.5	-	-	-	2426.1	860.1×10^{-3}	731	4004.2
E_{NACE}	27.5	2503.8	51.1	-	-	-	3716.2	849.7×10^{-3}	646	6247.5
-0.7 V	27.1	-	-	3319.0	813.1×10^{-3}	1322	6378.0	745.8×10^{-3}	4027	9724.1
-0.8 V	26.6	-	-	1206.4	815.5×10^{-3}	1311	13008.0	601.8×10^{-3}	2520	14241.0

that prolonged exposure led to surface changes affecting current demand. Nevertheless, the results exhibited a strong correlation, indicating that cathodic protection potentials and required current densities can be reliably estimated through calculations and simulations.

3.3 Verification of Cathodic Potentials

To investigate the surface characteristics and evaluate the effectiveness of the applied cathodic potentials, EIS tests were conducted. The Nyquist plots of CD100% at E_{corr}, E_{NACE}, -0.7, and -0.8 V are presented in **Figure 6(a)**. A depressed capacitive loop, which is commonly associated with charge transfer during the corrosion process, was observed at all cathodic potentials **[11][12]**. The semicircle diameter, representing charge transfer resistance (R_{ct}), increased as the cathodic potential became more negative, enabling a comparative assessment of corrosion resistance. In contrast, an inductive loop at low frequency was only observed at E_{corr}, E_{NACE}. The presence of this inductive loop indicates that the adsorption of intermediate species, such as metal hydroxides, oxygen species, or H^+_{ads}, is actively occurring. This suggests that insufficient cathodic protection at E_{corr} and E_{NACE} has led to the accumulation of corrosion products on the surface of CD100% **[13]**. Conversely, at -0.7 and -0.8 V, where no inductive loop was observed, the system appears to be under effective cathodic protection, minimizing surface adsorption effects and stabilizing the electrode-electrolyte interface.

As the distinct characteristics depending on the cathodic potentials were exhibited, different equivalent electrical circuit (EEC) models were used. The impedance parameters of CD100% at E_{corr} and E_{NACE} were identified using the EEC shown in Fig. 6 (b). The circuit consists of the following components: R_s represents the solution resistance; R_L and L correspond to the inductive elements; R_{ct} denotes the charge transfer resistance; and C_{dl} (CPE) signifies the double layer capacitance. To achieve a more accurate fit, a constant phase element (CPE) was introduced instead of an ideal capacitor **[12]**. The impedance parameters of CD100% at -0.7 and -0.8 V, which demonstrated sufficient cathodic protection, were determined using the electrical equivalent circuit model shown in **Figure 6(c)**. The circuit consists of the following components: R_s represents the solution resistance; R_{film} and C_{film} (CPE_1) denotes the electrical resistance and capacitance of the oxide film, respectively; R_{ct} is the charge transfer resistance; C_{dl} (CPE_2) is the double layer capacitance.

The CPE impedance is expressed as:

$$Z_{CPE} = \frac{1}{Y_0(j\omega)^n}$$

Where Y_0 is the magnitude of the CPE and n is the deviation from ideal capacitive behavior due to the surface roughness, porosity, or electrode heterogeneity **[14]**.

The conversion of the CPE to capacitance was performed using the equation below **[15]**:

$$C = Y_0(\omega_{max})^{n-1}$$

Where ω_{max} = $2\pi f_{max}$, f_{max} is the frequency where the imaginary part of the impedance reaches its maximum.

The impedance parameters of CD100% at E_{corr} and E_{NACE}, -0.7 and -0.8 V are listed in **Table 4**. It can be noted that R_{ct} increased as the cathodic protection potential became more negative. This aligns with the ICCP principle, where a more negative potential enhances the suppression of anodic dissolution by shifting the surface further into the cathodic region. As a result, R_{ct}, which represents the difficulty of electron transfer in corrosion reactions, increases due to the reduced corrosion activity and the stabilization of the passive film on the metal surface. The R_{film} at -0.7 V was larger than that at -0.8 V, indicating that the suppression of anodic reactions at more negative potentials reduced oxide film formation, thereby decreasing R_{film}.

The capacitance related to oxide film (C_{film}) and electrical double layer (C_{dl}) can be represented by:

$$C = \frac{\varepsilon\varepsilon_0 A}{d}$$

Where ε is the dielectric constant, ε_0 is the vacuum permittivity, A is the surface area of the electrode, and d is the thickness.

At cathodic protection potentials of -0.7 and -0.8 V, C_{film} showed nearly identical values, suggesting that the oxide film thickness was similar. This indicates that -0.7 V provides corrosion protection performance comparable to that of -0.8 V. C_{dl} at E_{corr} and E_{NACE} were lower than those at -0.7 and -0.8 V, which can be attributed to the increased corrosion reactions generating intermediate species. These species likely contributed to a thicker double layer, reducing the overall capacitance. On the other hand, the C_{dl} at -0.7 V was higher than that at -0.8 V. At more negative cathodic potentials, the cathodic reaction ($O_2 + 2H_2O + 4e^- \rightarrow 4OH^-$) becomes more dominant, leading to a greater concentration of ions at the electrode surface. As a result, the electrical double layer thickens, causing a reduction in C_{dl}.

To further evaluate the effectiveness of cathodic potentials, SEM/EDS analysis was performed on the surface of CD100% after the potentiostatic tests. As depicted in **Figure 7**, the surfaces of CD100% at -0.7 and -0.8 V remained clear, whereas corrosion products were observed on CD100% at E_{corr} and E_{NACE}. Additionally, EDS mapping revealed that the Fe content in CD100% was 58.9, 69.7, 91.9, and 94.3 at%, while the O content was 41.1, 30.3, 8.1, and 5.7 at% at E_{corr}, E_{NACE}, -0.7, and -0.8 V, respectively. The lower Fe content and higher O content observed at E_{corr} and E_{NACE} indicate extensive oxide film formation, suggesting significant corrosion. Therefore, -0.7 V and -0.8 V can be considered effective cathodic protection potentials. These findings are consistent with the calculated corrosion rates and EIS results, further confirming the effectiveness of the cathodic potentials.

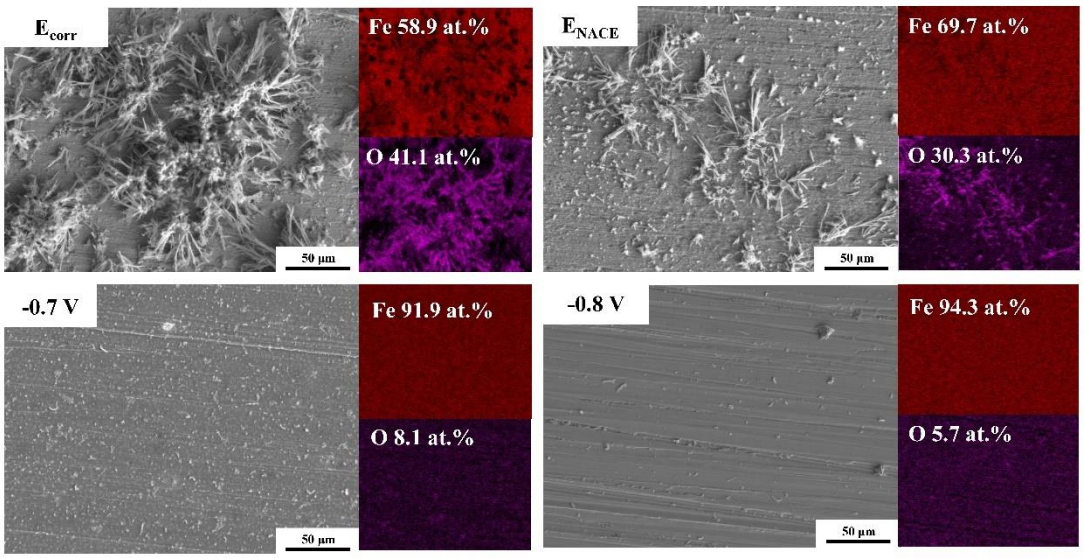

Figure 7: SEM images and EDS mapping of CD100% after potentiostatic tests

4. Conclusion

The efficient cathodic protection potentials and impressed current densities in ICCP systems for ships with coating defects were investigated through electrochemical analyses, computer simulations, and material characterization. The main findings are summarized as follows:

1. The corrosion rates of CD10%, CD30%, CD50%, and CD100% were 0.027, 0.050, 0.078, 0.137, and 0.235 mm/yr, respectively, exceeding the low corrosion rate threshold (0.025 mm/yr) recommended by NACE. This highlights the necessity of implementing ICCP systems to mitigate corrosion.
2. Cathodic protection potentials satisfying the low corrosion rate criterion proposed by NACE was estimated from the potentiodynamic polarization curves and the required current densities for the potentials were determined through calculations, simulations, and experiments. When the trend line was plotted based on the calculated values, the simulation and experimental results demonstrated strong correlations, with high R^2 of 0.996 and 0.962, respectively.
3. R_{ct} increased as the cathodic protection potential became more negative. In addition, no inductive loop was observed in the Nyquist plots at -0.7 and -0.8 V, whereas an inductive loop, indicative of active accumulation of corrosion products, appeared at E_{corr} and E_{NACE}. Furthermore, the oxide films generated at -0.7 and -0.8 V were significantly less pronounced than those at E_{corr} and E_{NACE}. These results suggest that -0.7 V also provides sufficient cathodic protection performance.

Acknowledgement

This research was supported by the Defense Acquisition Program Administration (DAPA) under the Defense Industry Component Localization Program (No. C220050).

Author Contributions

Conceptualization, U. Kim and S. Lee; Methodology, U. Kim; Software, U. Kim; Validation, U. Kim and S. Lee; Formal Analysis, U. Kim; Investigation, U. Kim, N. Kim; Resources, J. Sin, Y. Maeng, and S. Lee; Data Curation, U. Kim, N. Kim; Writing—Original Draft Preparation, U. Kim, N. Kim; Writing—Review & Editing, S. Lee; Visualization, U. Kim; Supervision, S. Lee; Project Administration, S. Lee; Funding Acquisition, J. Sin, Y. Maeng, and S. Lee.

References

[1] S. Yan, G. -L. Song, Z. Li, H. Wanh, D. Zheng, F. Cao, M. Horynova, M. S. Dargusch, and L. Zhou, “A state-of-the-art review on passivation and biofouling of Ti and its alloys in marine environments,” Journal of Materials Science & Technology, vol. 34, pp. 421-435, 2018.

[2] NACE International, Control of External Corrosion on Underground or Submerged Metallic Piping Systems, NACE International, 2013.

[3] D. N. Veritas, Cathodic Protection Design, Recommended Practice DNV-RP-B401, 2010.

[4] NACE International, Preparation, Installation, Analysis, and Interpretation of Corrosion Coupons in Oilfield Operations, NACE International, 2005.

[5] C. Thiel, C. Broecheler, F. Ludwar, A. Rennings, J. Doose, and D. Erni, “A simple superposition formulation to predict the underwater electric potential signature of naval vessels,” Journal of Marine Science and Engineering, vol. 8, pp. 105-116, 2020.

[6] C. Thiel, K. Neumann, F. Ludwar, A. Rennings, J. Doose, and D. Erni, “Coating damage localization of naval vessels using artificial neural networks,” Ocean Engineering, vol. 192, pp. 106560-106566, 2019.

[7] J. Wu, S. Xing, and F. Yun, “The influence of coating damage on the ICCP cathodic protection effect,” WIT Transactions on Engineering Sciences, vol. 65, pp. 89-96, 2009.

[8] E. Santana-Diaz and R. Adey, “Predicting the coating condition on ships using ICCP system data,” International Journal for Numerical Methods in Engineering, vol. 62, pp. 727-746, 2005.

[9] Corrosion Protection of a Ship Hull. Available: https://www.comsol.com/model/corrosion-protection-of-a-ship-hull-14565.

[10] ISO 12473:2017 General principles of cathodic protection in seawater. Available: https://www.iso.org/standard/67729.html.

[11] K. Lima, V. M. Palva, D. Perrone, B. Ripper, G. Simões, M. L. M. Rocco, A. G. Veiga, and E. D’Elia, “Glycine max meal extracts as corrosion inhibitor mild steel in sulphuric acid solution,” Journal of Materials Research and Technology, vol. 9, pp. 12756-12772, 2020.

[12] V. V. Torres, V. A. Rayol, M. Magalhães, G. M. Viana, L. C. S. Aguiar, S. P. Machado, H. Orofino, and E. D’Elia, “Study of thioureas derivatives synthesized from a green

route as corrosion inhibitors for mild steel in HCl solution," Corrosion Science, vol. 79, pp. 108-118, 2014.

[13] H. H. Hernández, A. N. R. Reynoso, H. C. T. González, C. O. G. Morán, J. G. M. Hernández, A. M. Ruiz, J. M. Hernández, and R. O. Cruz, "Electrochemical impedance spectroscopy (EIS): A review study of basic aspects of the corrosion mechanism applied to steels," Electrochemical Impedance Spectroscopy, pp. 137-144, 2020.

[14] M. Sluyters-Rehbach, "Impedances of electrochemical systems: Terminology, nomenclature and representation-Part I: Cells with metal electrodes and liquid solutions," Pure and Applied Chemistry, vol. 66, pp. 1831-1891, 1994.

[15] L. S. Rodrigues, A. F. Valle, and E. D'Elia, "Biomass of microalgae spirulina maxima as a corrosion inhibitor for 1020 carbon steel in acidic solution," International Journal of Electrochemical Science, vol. 13, pp. 6169-6189, 2018.